Runouts of landslide masses detached in the 2018 Hokkaido Eastern Iburi Earthquake

Kazuo KONAGAI[1], Alessandra Mayumi NAKATA[2]

[1]Fellow of JSCE, Professor Emeritus, University of Tokyo
(1-21-4-517 Wakaba, Shinjuku-ku, Tokyo 160-0011, Japan)
E-mail:kaz3776k@gmail.com
[2]Member of JSCE, Researcher, International Consortium on Landslides
(4-10-17-11 Nishihara, Kashiwa, Chiba 277-0885, Japan)
E-mail: amnakata@gmail.com

Key Facts
- Hazard Type: Earthquake
- Date of disaster: Sept. 6th, 2018
- Location of Survey: Iburi, Hokkaido, Japan
- Date of the field survey: Nov. 13th to 17th, 2018
- Survey tools: GPS receivers, UAV
- Key findings:
  1) Morphological features of 30 landslide masses in the epicentral area suggested that the activated average frictional coefficients on slip surfaces, μ_1, and flat rice fields, μ_2, could have been about 0.165 and 0. 36, respectively.
  2) However, μ_1 might have been even smaller than this value for smaller and gentler detached masses.

Key Words : *Hokkaido Eastern Iburi Earthquake, volcanic ash and pumice, landslides*

1. INTRODUCTION

The major impact of the M_w 6.6 September 6th, 2018 Hokkaido Eastern Iburi Earthquake was obviously in the form of geotechnical failures as described in the authors' previous report[1)]. The intense tremor triggered more than 3,300 landslides confirmed over an area of about 20 km × 20 km near Atsuma Town[2)], wiping out homes sparsely distributed along foothills of mountains. Around 80% of 41 victims were confirmed dead of suffocation[3)].

This calamity has left a big question about how far out a landslide mass can travel. Since the majority of more than 3,300 landslides in the epicentral area were shallow and planar masses of volcanic ash and pumice and they have deposited over extensive flat rice fields sometimes dotted with farm houses, a discussion is made herein about common geometrical features of these landslide masses, which is expected to provide a clue as to possible runout distances of these landslide masses.

2. DIMENSIONS OF LANDSLIDE MASSES AND RUNOUTS

Eruptions of major volcanoes such as Shikotsu (about 40,000 years ago), Tarumae (about 20,000 years ago) and Eniwa (about 9,000 years ago) have left layers of volcanic matters such as pumice draping the hilly landscape with sediments deposited on top later[4)]. These pumice-rich layers seem to have collapsed in the intense shake, and have caused the multiple landslides, which all look similar with each other in terms of color of the exposed bare earths, uprooted trees densely accumulated near the distal ends of landslide masses, etc. The noteworthy common features of these landslides are that (1) root systems that can help trees "grab onto" soil and keep it clumped together never penetrated through the pumice/ volcanic ash drape and stayed above the slip surfaces, and that (2) almost an entire body of each landslide mass has left the slope with little fraction of the mass remaining on the slope.

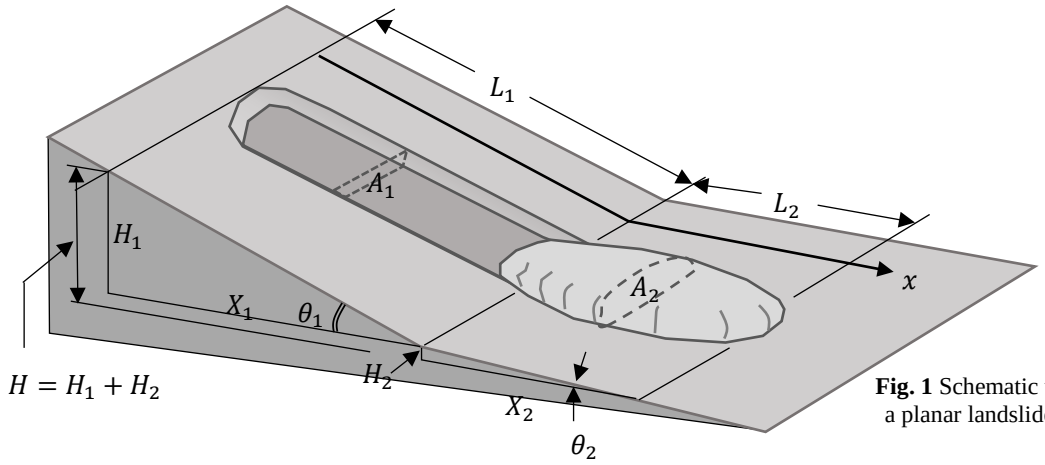

Fig. 1 Schematic view of a planar landslide mass

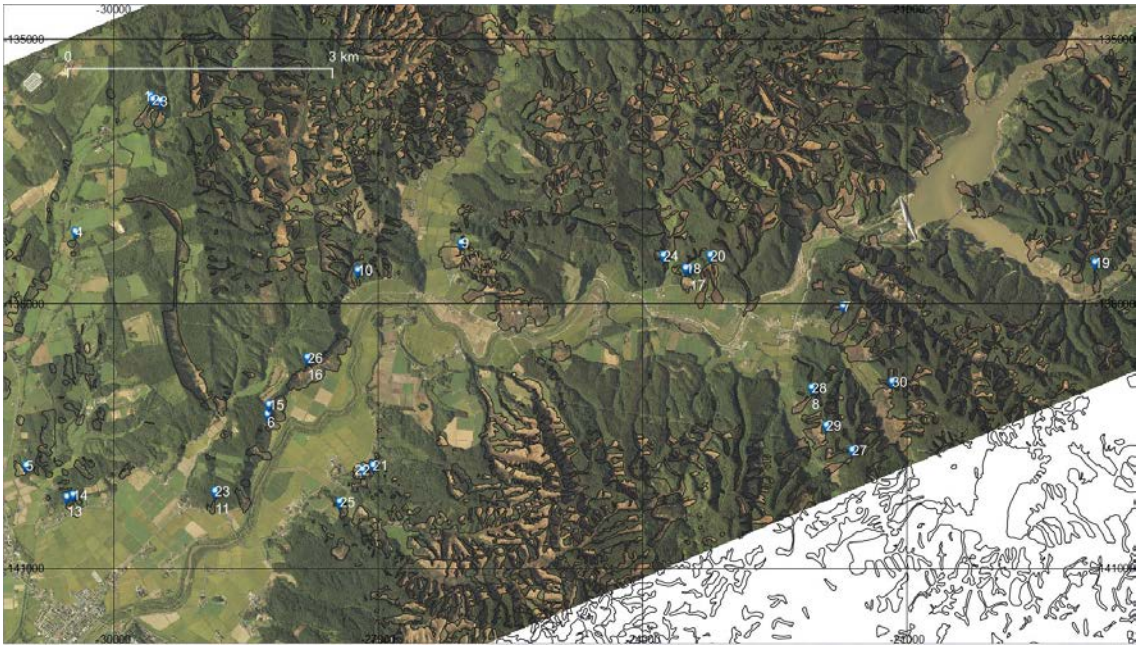

Fig. 2 Near Atsuma Town, 30 landslides dimensions were measured.

Given the abovementioned features of many landslides, we focus exclusively on independent landslide masses that traveled over flat rice fields. Sometimes, these masses that spread over the flatland are touching side by side with each other. However, as long as their interactions are not significant, we take them tentatively into targets of examination just to assure that the result can have some statistical significance.

A landslide mass with its initial length L_1 and cross-sectional area A_1 is assumed to have decelerated as it traveled over a flat land and stopped completely with its final length L_2 and cross-sectional area A_2 immediately when the whole mass left the slope L_1 (Fig. 1). The variations of A_1 and A_2 along the direction of the dip (x) are assumed to be substantially small and fluctuate little around their average values $\bar{A}_1$ and $\bar{A}_2$. Since the landslide mass does not change its mass M, $\rho_i \bar{A}_i L_i = M$ is kept constant where ρ_i , $\bar{A}_i$, and L_i are respectively density, average cross-sectional area and length of the landslide mass with $i =$ either 1 or 2 for the initial or the final stage of sliding. Total 30 landslide masses shown with blue place-marks in Fig. 2 were examined, and the dimensions of these landslide masses are listed in Table 1.

The work W_1 used up through friction exerted upon the sliding surface L_1 is given by:

$$W_1 = \int_0^{L_1} \rho_1 g A_1 (L_1 - x) \cos\theta_1 \, \mu_1 dx$$
$$= \rho_1 g \bar{A}_1 L_1 \cos\theta_1 \, \mu_1 \frac{L_1}{2}$$
$$= Mg \cos\theta_1 \, \mu_1 \frac{L_1}{2} \qquad (1)$$

where, g is the gravitational acceleration, $\cos\theta_1$ is the cosine of the average dip of the slope L_1, and is given by:

$$\cos\theta_1 = \frac{X_1}{L_1} \qquad (1a)$$

Table 1 Dimensions of 30 landslide masses shown in **Fig. 2**

ID	Location of top scar		L_1 (m)	L_2 (m)	H_1 (m)	H_2 (m)	H (m) (H_1+H_2)	X_1(m)	X_2(m)
	East Longitude (degree)	North Latitude (degree)							
1	141.8885	42.7776	205.3	108.6	72.1	13.3	85.3	192.2	107.8
2	141.8888	42.7772	156.3	106.5	64.3	2.3	66.6	142.5	106.5
3	141.8898	42.7770	120.7	101.4	40.8	8.8	49.5	113.6	101.0
4	141.8781	42.7636	87.9	14.6	12.3	0.2	12.5	87.1	14.6
5	141.8714	42.7398	70.5	46.5	24.9	-0.1	24.9	65.9	46.5
6	141.9048	42.7451	78.4	93.3	30.8	2.8	33.6	72.0	93.2
7	141.9846	42.7564	159.7	106.3	56.2	8.2	64.5	149.4	106.0
8	141.9803	42.7480	150.4	165.4	69.8	8.7	78.5	133.2	165.1
9	141.9316	42.7627	134.0	121.1	48.9	4.8	53.7	124.8	121.0
10	141.9172	42.7599	71.7	27.3	31.3	4.6	35.9	64.5	26.9
11	141.8976	42.7371	96.2	68.6	34.6	1.5	36.2	89.7	68.6
12	141.8743	42.7149	42.6	11.9	9.7	0.1	9.8	41.5	11.9
13	141.8771	42.7366	105.6	37.0	13.4	0.1	13.5	104.8	37.0
14	141.8779	42.7368	101.1	64.7	14.6	0.2	14.8	100.0	64.7
15	141.9050	42.7461	77.9	131.3	38.7	3.1	41.8	67.6	131.3
16	141.9104	42.7509	115.1	90.2	42.1	1.8	43.8	107.1	90.2
17	141.9633	42.7601	113.6	77.6	65.2	4.4	69.6	93.0	77.5
18	141.9627	42.7602	106.8	68.7	63.6	4.2	67.8	85.8	68.6
19	142.0194	42.7609	144.5	125.4	79.8	14.0	93.8	120.4	124.6
20	141.9661	42.7615	308.8	163.3	93.1	3.5	96.6	294.5	163.3
21	141.9195	42.7400	96.8	46.3	26.9	0.4	27.3	93.0	46.3
22	141.9180	42.7395	106.1	56.3	31.2	0.7	31.8	101.4	56.3
23	141.8976	42.7372	83.7	96.3	39.3	3.7	43.0	73.9	96.3
24	141.9596	42.7614	49.2	32.0	27.1	2.1	29.2	41.0	31.9
25	141.9149	42.7362	65.3	41.8	23.7	-0.1	23.5	60.8	41.8
26	141.9104	42.7509	116.1	85.2	42.8	1.0	43.8	107.9	85.2
27	141.9858	42.7417	189.7	159.8	86.6	4.0	90.6	168.8	159.8
28	141.9802	42.7480	152.0	159.3	71.2	8.3	79.5	134.4	159.1
29	141.9822	42.7442	110.9	85.9	58.3	3.7	62.0	94.4	85.8
30	141.9914	42.7487	99.0	141.5	54.8	4.3	59.0	82.5	141.5

μ_1 is the mobilized frictional coefficient on the sliding surface L_1, which is assumed to be uniform over the entire stretch of the slope. Likewise, the work W_2 used through friction exerted upon the depositional area L_2 is given by:

$$W_2 = \int_0^{L_2} \rho_2 g A_2 x \cos\theta_2 \, \mu_2 dx$$

$$= \rho_2 g \bar{A}_2 L_1 \cos\theta_2 \, \mu_2 \frac{L_2}{2} = Mg \cos\theta_2 \, \mu_2 \frac{L_2}{2} \quad (2)$$

where, $\cos\theta_2$ is given by:

$$\cos\theta_2 = \frac{X_2}{L_2} \quad (2a)$$

In addition to the above, there is an energy dissipation process in the interior of the deforming landslide mass to be sure, but this energy dissipation is assumed to be less significant than W_1 and W_2. Thus, the summation of these works is considered to be nearly equal to the initial potential energy of the landslide mass, which is given by:

$$E_p = \frac{MgH}{2} = \frac{Mg(H_1+H_2)}{2} \quad (3)$$

Equating Equation (3) with Equation (1) + Equation (2), one obtains:

$$H \cong \cos\theta_1 \, \mu_1 L_1 + \cos\theta_2 \, \mu_2 L_2$$

$$= \mu_1 X_1 + \mu_2 X_2 \quad (4)$$

If the variations of μ_1 and μ_2 within the epicentral area are substantially small and follow normal distributions, a multiple linear regression analysis for the relationship between the dependent variable H and two independent variables X_1 and X_2 with its intercept set at zero can give us the overall picture of the mobilized frictional coefficients.

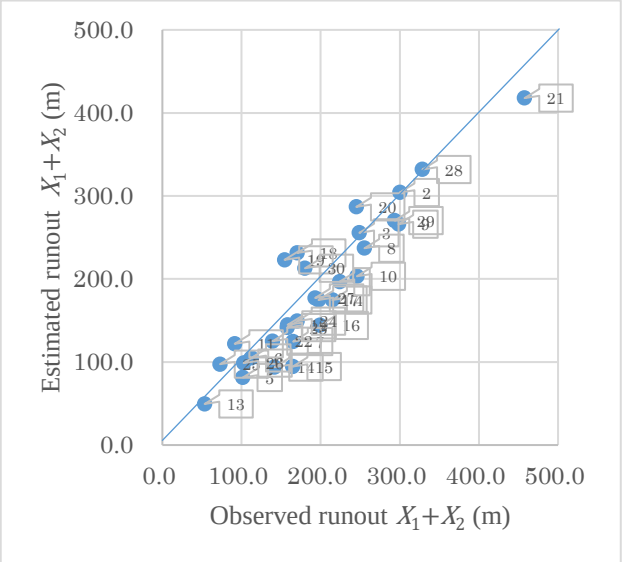

Fig. 3 Comparison of the observed and estimated runouts $X_1 + X_2$ values.

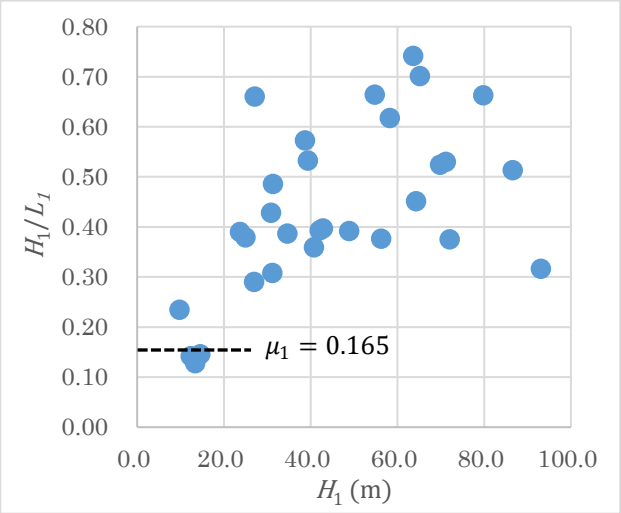

Fig. 4 Slope inclinations H_1/L_1 for different relative heights of top scars H_1

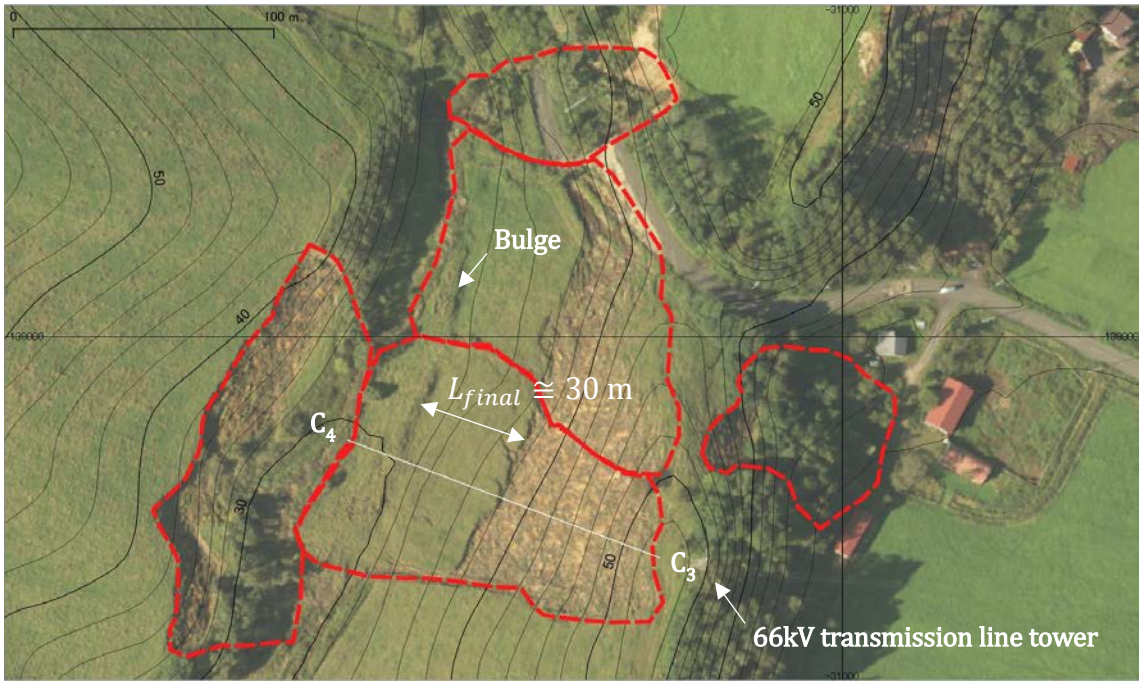

Fig. 5 Coherent landslide mass compressed against the other side wall of valley[1)]

For the 30 landslides (28 degrees of freedom) listed in Table 1, the average values of $\mu_1 = 0.165$ and $\mu_2 = 0.36$ were obtained with the standard errors of $\sigma_{\mu_1} = 0.058$ and $\sigma_{\mu_2} = 0.069$, respectively, and the coefficient of determination of 0.94. The average frictional coefficient $\mu_1 = 0.165$ on the slopes is less than a half of $\mu_2 = 0.36$ on the flat rice fields. Thus, runout distances $X_1 + X_2$ in this event can be predicted using the following equation:

$$X_1 + X_2 \cong \frac{H}{\mu_2} + \left(1 - \frac{\mu_1}{\mu_2}\right) X_1 = 2.8H + 0.54X_1 \cong 2.8H_1 + 0.54X_1 \quad (5)$$

Fig. 3 compares the observed and estimated runouts $X_1 + X_2$ for the 30 landslides. Though Equation (5) helps understand the overall image of devastation, it is perhaps premature to discuss each detail with the average values of μ_1 and μ_2 obtained from the 30 landslides, because there were no small number of slopes that have slipped even with their inclinations smaller than the average value of $\mu_1 = 0.165$. It is noted that many landslides including these gentle slopes are inevitably on the unsafe (right) side of the prediction line (Equation (5)) drawn on Fig. 3.

Fig. 4 plots slope inclinations H_1/L_1 of the chosen 30 landslides against the heights of their top scars H_1. As a whole, the smaller the H_1 values are, the smaller are the inclinations H_1/L_1, and three slopes are found

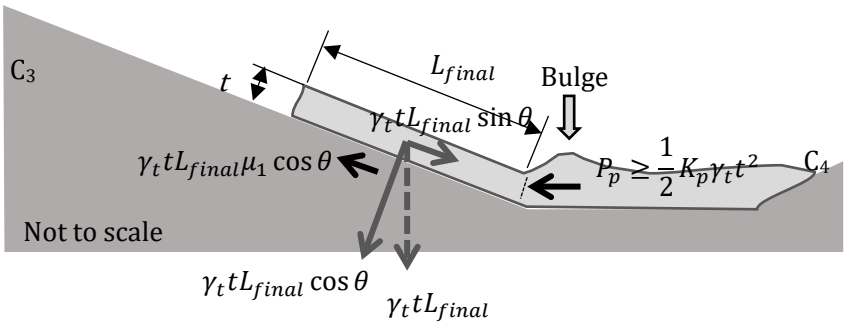

Fig. 6 Cross-section of landslide mass that has stopped moving being compressed against the other side wall of valley[1] (not to scale): Symbols have been replaced with the ones used in this report.

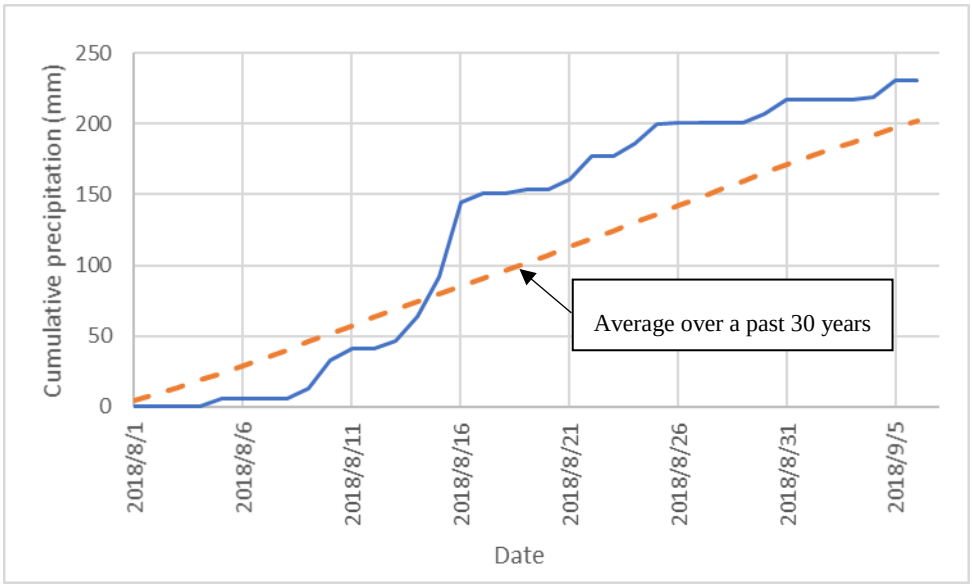

Fig. 7 Cumulative precipitation at Atsuma JMA Observatory for the period from August 1 to September 6, 2018 (Data from the Japan Meteorological Agency[5])

below the $H_1/L_1 = 0.165$ line in this figure. In the authors' previous report[1], μ_1 was examined using a small landslide on a very gentle slope shown in Fig. 5 with $H_1 \cong 20$ m and $H_1/L_1 \cong 0.2$. This planar landslide mass, after sliding on this gentle slope, hit the opposite wall of the shallow valley and formed a transverse bulge as illustrated in Fig. 6. This bulge was assumed to have developed where wedges of passive soil failure formed one after another at the boundary between the toe part pressed against the opposite valley wall and the slowing tail part with the uniform thickness t as illustrated in Fig. 6. This tail part was gradually shortening until its final length of L_{final} was reached. Given this assumption, μ_1 was obtained to be 0.05 as much.

The gentler and the smaller slopes are, the wetter they may have been, because the greater parts of slip surfaces formed in the small and gentle slopes could have been well beneath the seepage lines, given the cumulative precipitation in the epicentral area (at Atsuma JMA Observatory) for the period from August 1 to September 6, 2018 (the date of the earthquake), exceeding the average for the same period over a past 30 years (1981 - 2010) by about 50 mm (Fig. 7). Further in-depth studies will be necessary to make use of the lessons from this earthquake.

4. SUMMARY

The noteworthy common features of almost all landslides in the epicentral area of the 2018 Hokkaido Eastern Iburi Earthquake are that (1) root systems that can help trees "grab onto" soil and keep it clumped together never penetrated through the pumice/ volcanic ash drape and stayed above the slip surfaces, and that (2) almost an entire body of each landslide mass deposited over a flat land with little fraction of the mass remained on the slope. Given these common features, dimensions of landslide masses that have deposited over flat rice fields have been examined. A multiple linear regression analysis for the relationship among the measured dimensions of total 30 landslide masses have given us both the average values of activated frictional coefficients $\mu_1 = 0.165$ on the slip surfaces and $\mu_2 = 0.36$ on the flat rice fields. However, the value of μ_1 for a smaller and gentler slope, which might have been wetter than the others, could have been even smaller

than this value. Further in-depth studies will be necessary for discussing possible runouts.

ACKNOWLEDGEMENT: The authors have jointly conducted this field survey with the team of lifeline earthquake engineering experts of the American Society of Civil Engineers (ASCE) led by Mr. John Eidinger and Mr. Alex Tang. The authors are indebted to Mr. Masataka Shiga, PhD candidate at the University of Tokyo, who have joined the field survey and helped the authors flying a UAV to collect 3D images of terrains. The authors would like to express their sincere thanks to Dr. Yukihiro Tsukada, Executive Director of the Japan Society of Civil Engineers (JSCE hereafter), Dr. Takanobu Suzuki, Chairman, Dr. Yoshihisa Maruyama, Secretary General and all members of the Subcommittee of Lifeline Earthquake Engineering, JSCE Committee of Earthquake Engineering, Mr. Satoshi Suenaga, Kubota Corp., and Mr. Jiro Nakamura, Chubu Electric Power Co., Inc., for their generous supports to this joint survey. The authors' field survey was partially supported by the Grant-in-Aid for Scientific Research (A), No. 16H02744.

REFERENCES

1) Kazuo KONAGAI, Seiji NISHIYAMA, Kanta OHISHI, Daiki KODAMA, Yuki NANNO: Large ground deformations caused by the 2018 Hokkaido Eastern Iburi Earthquake, JSCE Journal of Disaster FactSheets, FS2018-E-0003, 1-8, 2018, http://committees.jsce.or.jp/disaster/system/files/FS2018-E0003.pdf.
2) Geographical Information Authority of Japan: Landslide map on GeoJSON format for the epicentral area of the 2018 Hokkaido Eastern Iburi Earthquake, Sept. 19, 2018, (in Japanese), http://www.gsi.go.jp/common/000204728.zip.
3) Fire and Disaster Management Agency: The 31st disaster report of the 2018 Hokkaido Eastern Iburi Earthquake, Sept. 19, 2018, and actions that FDMA has taken so far, Oct. 11, 2018, (in Japanese), http://www.fdma.go.jp/bn/2018/detail/1074.html.
4) Geological Survey of Japan, AIST: Characteristics of pyroclastic deposit from Shikotsu quaternary eruptions, 2018, (in Japanese), https://www.gsj.jp/hazards/earthquake/hokkaido2018/hokkaido2018-05.html.
5) Weather record retrieving site, Japan Meteorological Agency, (in Japanese), https://www.data.jma.go.jp/obd/stats/etrn/index.php.

(Received Dec. 14, 2018)